Identification of the two-degree-of-freedom system for heave motion responses of twin hulls with a moonpool

Sheng-Chao JIANG (姜胜超)[a*], Wei BAI (柏威)[b], Hao LIU (刘浩)[a], Yong-Qiang Huang[c], Jun-Jie LAN (兰俊杰)[d]

a. State Key Laboratory of Coastal and Offshore Engineering, Dalian University of Technology, Dalian 116024, China
b. Department of Computing and Mathematics, Manchester Metropolitan University, Chester Street, Manchester M1 5GD, UK
c. Dalian Shipbuilding Industry Co., Ltd, Dalian 116024, China
d. Power China Huadong Engineering Corporation Limited, Hangzhou, 311122, China

**Corresponding author*
Email address: jiangshengchao@foxmail.com (Sheng-Chao JIANG)

ABSTRACT

The heave motion response of the hulls is significantly affected by the fluid resonance in the moonpool, where the two-peak variation with the incident wave frequency is the most important phenomenon. Theoretical analysis based on the potential flow model is developed in the present work to identify the physics of the two-peak phenomenon. A conceptual model is also established to reveal the essential mechanics of the two peaks. It is disclosed that the heave motion response and free surface oscillation are essentially a two-degree-of-freedom system with the main and attached spring oscillators. The two peaks are the first and second resonant frequencies of the system with the in-phase and out-of-phase resonant modes, respectively. A new approach to the free decay test is also proposed to determine the resonant frequencies and resonant modes.

Keywords: Moonpool, coupling action, heave motion, fluid resonance, resonant frequency, resonant mode.

Introduction. For twin hulls with a moonpool, there are strong coupling actions between the heave motion response of the hulls and the free surface oscillation in the moonpool. On the one hand, the free surface oscillation in the moonpool shows a two-peak variation with the incident wave frequency. On the other hand, the heave motion response of the hulls is also typically characterized by two peaks and a tough over a range of incident wave frequencies (Ravinthrakumar et al., 2020; Gao et al., 2021; Jing et al., 2024). However, the interpretation of physical mechanisms behind the above phenomena is not conclusive. Ding et al. (2022) considered that the two peaks are the "natural frequency of the heave motion" and "natural frequency of the gap flow" at the low-frequency and high-frequency ranges, respectively. Lu et al. (2020) and Jiang et al. (2024) defined the two peaks as the first and second peak frequencies in their work. This, in fact, is a reservation on the physics of the two-peak phenomena. In this study, the physics behind the two-peak responses is revealed. According to the potential flow simulation and conceptual model, the interaction between the heave motion and fluid oscillation is interpreted by a coupled system of main-attached oscillators. The observed two-peak phenomena are explained by the first and second resonant frequencies and resonant modes of the adopted coupled system. Finally, a new approach to the free decay test based on CFD simulations is proposed in this study to determine the resonant frequencies and resonant modes. The present work is an important extension to the work reported in Jiang et al. (2024).

Potential flow model. The potential flow model in the frequency domain is used for simulating the coupling action between the heave motion response of the hulls and the free surface oscillation in the moonpool. The equation of floater motion response ξ can be defined as follows,

$$[-\omega^2(\mathbf{M}+\mathbf{A})-\mathrm{i}\omega(\mathbf{B}+\mathbf{V})+(\mathbf{C}+\mathbf{K})]\{\xi\}=[\mathbf{F}] \quad (1)$$

where ω is the circular frequency of both the incident wave and the floater motion response, and **M** is the total mass matrix of the floater. **F**, **A**, **B** and **C** are the are the exciting force, added mass matrix, radiation damping matrix and restoring force matrix, respectively, which include the influence of free surface oscillations in the moonpool. **V** and **K** are the viscous damping and stiffness matrices, respectively. Note that the potential flow model is solved numerically by using a higher-order boundary element method. In this work, the potential flow model is adopted to support the analysis of resonant periods in the coupled system.

Viscous fluid flow model. A viscous numerical wave flume based on the Navier-Stokes (NS) equations is also utilised in this study, where the OpenFOAM package is adopted for the simulations. In the Arbitrary Lagrangian-Eulerian (ALE) reference system, the governing equations are,

$$\frac{\partial\rho}{\partial t}+\frac{\partial\rho u_i}{\partial x_i}=0, \quad (2a)$$

$$\frac{\partial\rho u_i}{\partial t}+\frac{\partial\rho(u_j-u_j^m)u_i}{\partial x_j}=\rho g_i-\frac{\partial p}{\partial x_i}+\mu_e\frac{\partial}{\partial x_j}\left(\frac{\partial u_i}{\partial x_j}+\frac{\partial u_j}{\partial x_i}\right), \quad (2b)$$

where x_i and u_i are Cartesian coordinate component and the fluid velocity component in the ith direction, respectively; u_i^m is the velocity component due to mesh deformation in the ALE frame. g_i is the gravitational acceleration; p is the fluid pressure. ρ and μ_e are the fluid density and effective dynamic viscosity, respectively. $\mu_e = \mu_m + \mu_t$, μ_m is fluid molecule viscosity and μ_t is turbulent viscosity.

The Re-Normalization Group (RNG) k-ε two-equation formulations are selected for closing the governing equations. The Volume of Fluid (VOF) method is adopted to track the fluid and capture the free surface motion. Details of the present CFD model can be found in our previous publication Jiang et al. (2024), including the mesh convergent test and numerical validations. Finally, the use of viscous numerical wave flume is mainly for the proposed free decay test in the present study.

General behaviour of heave motion response and free surface oscillation. Following our previous work in Jiang et al. (2024), the two-dimensional steady-state free surface oscillation in the moonpool and the heave motion response of twin hulls with the vertical mooring stiffness are considered, as shown in Fig. 1. The twin hulls with the breadth $B = 2B_L = 0.720$ m and height $B_H = 0.360$ m, and the moonpool with the breadth $B_{mp} = 0.180$ m and draft $D = 0.180$ m, in the water depth $h = 1.030$ m, are selected, where the twin hulls are rigidly connected and only the heave motion is free. Note that the vertical restoring force coefficient of the two-hull structure is $k = 7200$ N/m, therefore, six different vertical stiffnesses around the value of $k = 7000$ N/m, which are $k = 0$, 1000, 4000, 7000, 14000 and ∞ (N/m), are considered in this study, and the incident wave height is $H_i = 0.03$ m in the viscous fluid flow simulations.

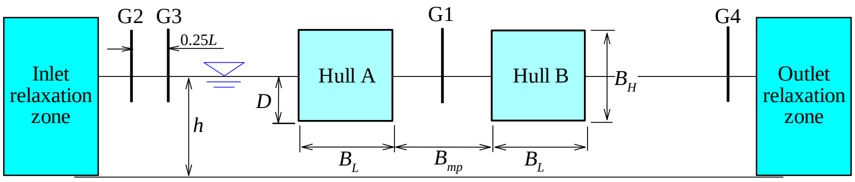

Figure 1: Sketch of the numerical wave flume with two identical hulls (quoted Fig. 1 in Jiang et al. (2024)).

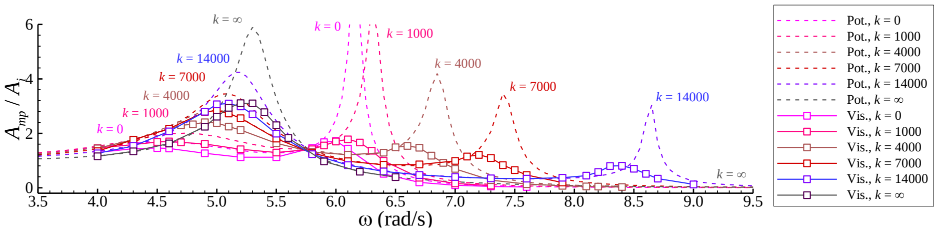

(a) Free surface oscillation

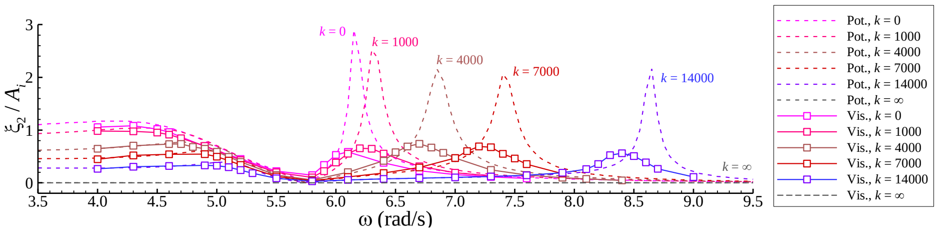

(b) Heave motion response

Figure 2: Variation of heave motion response and free surface oscillation against the incident wave frequency with different vertical mooring stiffnesses (quoted Fig. 7 in Jiang et al. (2024)).

Fig. 2 shows the variation of the free surface oscillation A_{mp} / A_i in the moonpool and the heave motion response ξ_2 / A_i of the hulls against the incident wave frequency, including the influence of the vertical mooring stiffness k. Potential flow results show the two-peak variation of the free surface amplitude in the moonpool with the incident wave frequency in the cases of non-fixed twin hulls, as shown in Fig. 2a. One of the peaks is smooth and bounded at the low-frequency range, which is defined as the first peak frequency $\omega_p^{(1)}$; while the other is a sharp spike at the high-frequency range, which is defined as the second peak frequency $\omega_p^{(2)}$. The two-peak variation can also be found in the heave motion response in Fig. 2b, although the peak value around the first peak frequency $\omega_p^{(1)}$ is a little hard to identify. In addition, there is a trough in the heave motion response in Fig. 2b, which is denoted as ω_s in this study. Numerical simulations suggest that $\omega_s = 5.80$ rad/s applies to all the vertical stiffnesses considered. The above behaviour is also noticed in the results of the viscous fluid flow modelling, indicating that it is a real physical phenomenon for the coupling actions between the heave motion response of the hulls and the free surface oscillation in the moonpool. Tab. 1 tabulates the major characteristic frequencies, ω_s, $\omega_p^{(1)}$ and $\omega_p^{(2)}$, in this study. Revealing their physics is the motivation of this study. In addition, the natural frequency $\omega_{rf} = 5.30$ rad/s of the fluid resonance in the moonpool formed by two fixed hulls is also included in the table, which is helpful for the following analysis.

Table 1 Definition of characteristic frequencies in this study.

Parameters	Definition of characteristic frequencies in this study	Value (rad/s)
$\omega_p^{(1)}$	Frequency of the first peak value	4.55 - 5.30
$\omega_p^{(2)}$	Frequency of the second peak value	6.15 - ∞
ω_s	Frequency of the zero heave motion response	5.80
ω_{rf}	Natural frequency of fluid resonance in fixed twin hulls	5.30

Identification of resonant frequencies of coupling system. The two-peak variation is the most important phenomenon in the coupling action between the heave motion response of the hulls and the free surface oscillation in the moonpool, which has been reported in many references (Ravinthrakumar et al., 2020; Lu et al., 2020; Gao et al., 2021; Jing et al., 2024; Jiang et al., 2024). However, none of these works reasonably explained the physics of the two peaks. It is believed that the two peaks should have a clear physical meaning, which is discussed in this section.

Based on the motion equation (1), the resonant frequency of the heave motion response of the hulls can be evaluated as,

$$\omega_r = \sqrt{\frac{C_{22}+K_{22}}{M_{22}+A_{22}(\omega_r)}}, \tag{3}$$

where ω_r is the resonant frequency of the heave motion response. In the equation, the restoring force C_{22} is independent of the angular frequency, while the added mass $A_{22}(\omega)$ is strongly dependent on the angular frequency, especially when the large-amplitude free surface oscillation in the moonpool happens. Using a suitable iteration procedure, the resonant frequency ω_r can be obtained.

Equation (3) is the solution of the resonant frequency without the damping effect. Based on Equation (1), the resonant frequency with the radiation damping effect can also be derived as,

$$\omega_d = \omega_r \sqrt{1-\mu_{22}^2(\omega)}, \tag{4}$$

where ω_d is the resonant frequency with considering the radiation damping. $\mu_{22}(\omega)$ is the damping ratio induced by the radiation damping in the heave motion direction, that is,

$$\mu_{22}(\omega) = \frac{B_{22}(\omega)}{2\sqrt{(M_{22}+A_{22}(\omega))(K_{22}+C_{22})}}, \tag{5}$$

where $B_{22}(\omega)$ is the main diagonal elements of the radiation damping matrix in the heave motion direction. Substituting Equations (3) and (5) into Equation (4), it has,

$$\omega_d = \frac{\sqrt{4C_{22}[M_{22}+A_{22}(\omega)]-B_{22}^2(\omega)}}{2[M_{22}+A_{22}(\omega)]}. \tag{6}$$

By solving Equations (3) and (6), the heave motion resonant frequencies of the hulls without and with the radiation damping effect are readily obtained, respectively. It should be noted that the influence of the free surface oscillation in the moonpool is already included in these equations according to the added mass $A_{22}(\omega)$ and the radiation damping $B_{22}(\omega)$.

Figure 3 shows the variations of the left-hand and right-hand terms of Equations (3) and (6) against the incident wave frequency, where the case of the hulls without the vertical stiffness ($k = 0$) is selected. The left-hand term ω is denoted by the solid black line, while the right-hand terms of Equations (3) and (6) are denoted by the dashed red line and solid blue line, respectively. The right-hand terms can be evaluated by the potential flow model, with $(K/M)_r^{1/2}$ for the cases without the radiation damping effect by Equation (3) and $(K/M)_d^{1/2}$ for the cases with the radiation damping effect by Equation (6). It can be observed that both $(K/M)_r^{1/2}$ and $(K/M)_d^{1/2}$ have two branches, which is attributed mainly to the significant variation of the added mass and radiation damping induced by the fluid resonance in the moonpool. The comparison between $(K/M)_r^{1/2}$ and $(K/M)_d^{1/2}$ indicates that the radiation damping has a significant effect on the low-frequency branch, while it is insignificant on the high-frequency branch. Therefore, the influence of the radiation damping should be considered when evaluating the heave motion resonant frequencies.

Furthermore, two intersections between the curves of the left-hand term ω and the right-hand term $(K/M)_d^{1/2}$ can be observed in the figure, indicating that Equation (6) has two roots, and hence the heave motion of the hulls with a moonpool has two resonant frequencies. Quantitative comparisons also confirm that the two roots in Figure 3 are exactly the previously identified $\omega_p^{(1)}$ and $\omega_p^{(2)}$ in Figure 2. This concludes that $\omega_p^{(1)}$ and $\omega_p^{(2)}$ are essentially the two heave resonant frequencies of the hulls coupling with the fluid resonance in the moonpool. Therefore, $\omega_p^{(1)}$ and $\omega_p^{(2)}$ are further defined as the first heave resonant frequency and the second heave resonant frequency of the hulls with a moonpool, respectively.

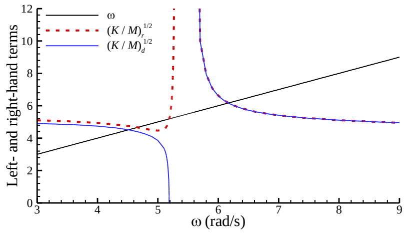

Figure 3: Theoretical solutions for heave motion resonant frequencies of the hulls with a moonpool.

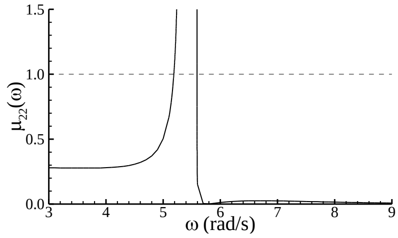

Figure 4: Damping ratio by the radiation damping.

Figure 4 shows the variation of the damping ratio of the heave hulls with the incident wave frequency. The damping ratio is calculated by Equation (5), that is, only the contribution of the radiation damping is considered. A dramatic increase in damping ratio $\mu_{22}(\omega)$ appears around the incident wave frequency ω_{rf} = 5.30 rad/s, which is the resonant frequency of fluid oscillation in the moonpool formed by the fixed twin hulls. Based on Equation (5), the increase in damping ratio comes from the increase of radiation damping $B_{22}(\omega)$ and the decrease of added mass $A_{22}(\omega)$, which can be confirmed by the results in Figure 5. It is worth noting that the value of $(M_{22} + A_{22})$ is negative around ω_{rf} = 5.30 rad/s, leading to that the damping ratio $\mu_{22}(\omega)$ gives rise to infinite on the occasion. Furthermore, Figure 4 also indicates that the values of damping ratios at the first and second heave resonant frequencies are $\mu_{22}(\omega_p^{(1)})$ = 0.281 and $\mu_{22}(\omega_p^{(2)})$ = 0.018, respectively. This explains that the peak value at the first heave resonant frequency is hard to identify, while the peak value at the second heave resonant frequency is remarkable in the potential flow model, as shown in Figure 2*b*.

At the frequency ω_s = 5.80 rad/s, the zero value of the heave motion amplitude can be observed in Figure 2*b*. This can be explained by Figure 5 that the exciting force, added mass and radiation damping are all zero at this frequency. The zero value of the exciting force can be understood by the ratio of wavelength and twin-hull breadth, which is $\lambda / (2B_L + B_{mp})$ = 2.08. The vertical wave forces generated by the wave crest and wave trough are generally cancelled with each other at this frequency. Furthermore, there is a Haskind - Hanaoka relationship for the exciting force and the hydrodynamic coefficients including the added mass and radiation damping in the potential flow model, where the exciting force can be expressed by the radiation potential (Newman, 1960). It determines that the zero values of the exciting force, added mass and radiation damping happen at the same frequency. Furthermore, the exciting force and hydrodynamic coefficients in Figure 5 are independent of the vertical stiffness, which is the reason for the zero heave motion amplitude at ω_s = 5.80 rad/s appearing in all of the vertical stiffnesses. In fact, the zero value may also be explained by a deeper understanding based on the vibration mechanics, including that the frequency ω_s = 5.80 rad/s is a little larger than the frequency ω_{rf} = 5.30 rad/s. This will be further discussed in the conceptual model in Section 5.

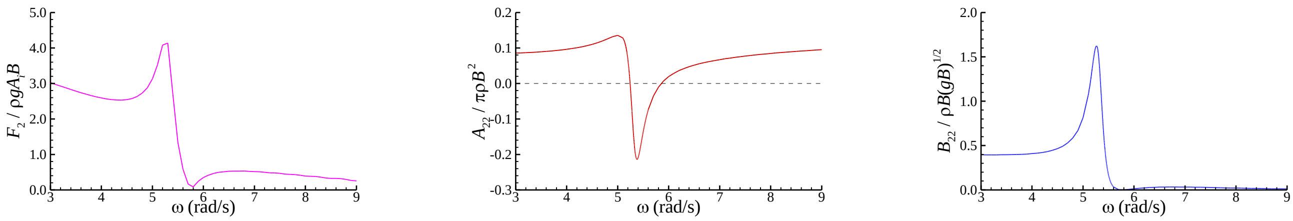

(a) Exciting force (b) Added mass (c) Radiation damping

Figure 5: Hydrodynamic coefficients of the hulls with a moonpool inside.

Figure 6 shows the influence of the vertical stiffness on the heave motion resonant frequencies of the hulls with a moonpool. The increase of vertical stiffness leads to the increase of $(K/M)_d^{1/2}$, which can be explained by Equation (6). A noteworthy feature is that the intersection between the left-hand term ω and the low-frequency branch of the right-hand term $(K/M)_d^{1/2}$ has a limit value ω_d = 5.20 rad/s. This is due to the dramatic increase of the damping ratio at this frequency, as shown in Figure 4. According to the analysis in this section, it can be confirmed that the two peaks are the first heave resonant frequency and the second heave resonant frequency of the hulls with a moonpool, respectively. The present theoretical method based on Equation (6) can work well in revealing the physics and predicting the resonant frequencies.

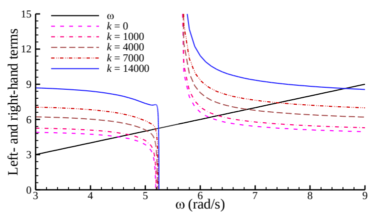

Figure 6: Influence of the vertical stiffness on the heave motion resonant frequencies of the hulls with a moonpool.

Theoretical analysis of resonant modes. The theoretical analysis in Section 4 indicates that there are two resonant frequencies. However, there are, in fact, some troubles with the basic theory of vibration mechanics. In this work, only the heave motion is free for the hulls, that is, this is a one-degree-of-freedom motion system. As well known, the one-degree-of-freedom motion system should only have one resonant frequency. To study this topic, a conceptual model is introduced to provide a qualitative interpretation.

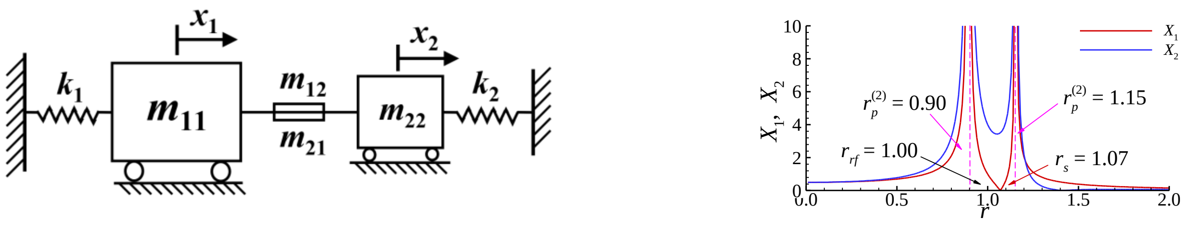

(a) Conceptual model

(b) Typical solutions

Figure 7: Sketch and typical solutions of the conceptual model for the system of main-attached spring oscillators with the coupling mass items m_{12} and m_{21}.

As shown in Fig. 7*a*, a system of two spring oscillators is adopted for describing the present coupled system of heave hulls with fluid response in the moonpool. The hulls are idealized by a main spring oscillator with the mass m_{11} and stiffness k_1 subjected to a harmonic excitation $F_1\sin\omega t$, and the fluid in the moonpool is represented by an attached spring oscillator with the mass m_{22} and stiffness k_2 subjected to a harmonic excitation $F_2\sin\omega t$. In difference to classical vibration mechanics, the interactions between the main and attached spring oscillators are affected by the added mass rather than the stiffness. That is, the non-diagonal elements of the stiffness matrix k_{12} and k_{21} are zero, while the non-diagonal elements of the mass matrix m_{12} and m_{21} are non-zero. That is, the two-spring system has the coupling mass items m_{12} and m_{21}. With neglecting the damping effect, the equations of motion response for the system are,

$$m_{11}\ddot{x}_1 + m_{12}\ddot{x}_2 + k_1 x_1 = F_1 \sin\omega t, \tag{7a}$$

$$m_{21}\ddot{x}_1 + m_{22}\ddot{x}_2 + k_2 x_2 = F_2 \sin\omega t. \tag{7b}$$

Only the steady-state solutions of the system are considered, so that,

$$x_{1p} = X_1 \sin\omega t, \tag{8a}$$

$$x_{2p} = X_2 \sin\omega t, \tag{8b}$$

where X_1 and X_2 are the amplitudes of the main and attached spring oscillators, respectively. Substituting Equation (8) into Equation (7), we have the following solutions,

$$X_1 = \frac{(k_2 - \omega^2 m_{22})F_1 + \omega^2 m_{12} F_2}{(k_1 - \omega^2 m_{11})(k_2 - \omega^2 m_{22}) - \omega^4 m_{12} m_{21}}, \tag{9a}$$

$$X_2 = \frac{\omega^2 m_{21} F_1 + (k_1 - \omega^2 m_{11})F_2}{(k_1 - \omega^2 m_{11})(k_2 - \omega^2 m_{22}) - \omega^4 m_{12} m_{21}}. \tag{9b}$$

In Equation (9), the amplitudes X_1 and X_2 give rise to infinite if the denominators of Equations (9a) and (9b) vanish. The two-root results for ω^2 are given in Equation (10),

$$(\omega^2)_{1,2} = \frac{(m_{22}k_1 + m_{11}k_2) \mp \sqrt{(m_{22}k_1 - m_{11}k_2)^2 - 4m_{12}m_{21}k_1k_2}}{2(m_{11}m_{22} - m_{12}m_{21})}. \tag{10}$$

The two roots are physically the two resonant frequencies of the coupled system, which explains the physics behind the two-peak responses observed in Figure 2, including the heave motion response and free surface oscillation.

The amplitude X_1 of the main spring oscillator vanishes when the numerator becomes zero. Since $(k_2 - \omega^2 m_{22})$ is included in the numerator of Equation (9a), it is speculated that the excitation frequency ω is close but unequal to the natural frequencies of the attached spring oscillation $(k_2/m_{22})^{1/2}$. The natural frequency of the attached spring oscillator in the conceptual model corresponds to the natural frequency ω_{rf} of the fluid resonance in the moonpool. This can be adopted to understand the zero heave motion response of the hulls at the frequency ω_s in Figure 2*b*, where the frequency ω_s is close but unequal to the frequency ω_{rf}. Furthermore, the numerator of Equation (9a) is independent of the stiffness k_1 of the main spring oscillator. That is, the corresponding frequency of the zero amplitude $X_1 = 0$ of the main spring oscillator is suitable for any stiffness k_1. It is also in accordance with the results that the zero heave motion amplitude ξ_2 / A_i always appears at the frequency $\omega_s = 5.80$ rad/s in all of the vertical stiffnesses in Figure 2*b*.

To better understand the conceptual model of main-attached spring oscillators, the following parameters are introduced,

$$\omega_{11} = \sqrt{k_1 / m_{11}}, \qquad \omega_{22} = \sqrt{k_2 / m_{22}}, \qquad r_1 = \omega / \omega_{11}, \qquad r_2 = \omega / \omega_{22},$$
$$\lambda = m_{22} / m_{11}, \quad \mu_{12} = m_{12} / m_{22}, \quad \mu_{21} = m_{21} / m_{22}, \quad \kappa = k_2 / k_1, \quad \varepsilon = F_2 / F_1$$

The parameters $\lambda = \kappa = \varepsilon = 0.25$ and $\mu_{12} = \mu_{21} = 0.5$, which determine $r_1 = r_2 = r$, are selected. Noted that these values have some similar with the present heave motion coupling moonpool problem. Fig. 7*b* shows the variation of the magnitudes of X_1 and X_2 with the external harmonic exciting frequencies. As expected, the magnitudes of X_1 and X_2 approach to infinity at the first and second resonant frequencies of $r_p^{(1)} = 0.90$ and $r_p^{(2)} = 1.15$ based on Equation (10) and decrease as r moves away from the resonant frequencies. The response amplitude of the main spring oscillator X_1 is zero at the frequency $r_s = 1.07$, which is close but a little larger than the natural frequency of the attached spring oscillator $r_{rf} = 1.0$. This is similar to the relationship between $\omega_{rf} = 5.30$ rad/s and $\omega_s = 5.80$ rad/s discussed above.

It can also be inferred from Equations (9a) and (9b) that X_1 and X_2 are of the same and opposite signs for $r < 1.07$ and $r > 1.07$ respectively, which suggests that the main and attached spring oscillators are in-phase and out-of-phase for $r < 1.07$ and $r > 1.07$ respectively. More specially, the main and attached spring oscillators are in-phase and out-of-phase at the first and second resonant frequencies of $r_p^{(1)} = 0.90$ and $r_p^{(2)} = 1.15$, respectively. The in-phase and out-of-phase relationships also correspond to the first and second resonant modes of the coupled system of main-attached spring oscillators. According to the above analysis, it can be speculated that the heave motion of the hulls and the fluid oscillation in the moonpool are essentially a two-degree-of-freedom motion system, which correspond to the main and attached spring oscillators, respectively. The first and second resonant modes of the coupled system of heave motion and fluid oscillation are the in-phase and out-of-phase relationships, respectively.

Finally, it should be noted that the definition of main and attached spring oscillators is from the large difference in mass between the two spring oscillators in this work. As illustrated in Fig. 7*b*, the ratio of mass $\lambda = m_{22} / m_{11} = 0.25$, indicating that the main oscillator has a much larger mass than the attached oscillator. Therefore, the hulls are idealized by a main oscillator and the fluid in the moonpool is represented by an attached oscillator. The mass ratio is also one of the major reasons for the zero value of X_1 at $r = 1.07$. Furthermore, the amplitudes X_2 of the attached oscillator also have a zero value, which can be confirmed by the analytical solutions of Equation (9b) and the result in Fig. 7*b* at $r = 1.40$.

Free decay tests and resonant modes. Free decay tests have been extensively adopted to capture the resonant frequency of floater motions, including the heave motion response. It has also been employed in the problem of heave motion of floaters with moonpool by many researches (Ding et al., 2022; Jing et al., 2024), but the previous work failed to give a clear explanation on the two peaks and the corresponding physics. A numerical free decay test based on CFD simulations is adopted in this study. The vertical stiffness $k = 7000$ N/m is selected, for which the first and second resonant frequencies are $\omega_p^{(1)} = 5.10$ rad/s and $\omega_p^{(2)} = 7.40$ rad/s, respectively. Two sets of initial conditions, these are, the initial heave amplitude of the hulls with $\xi_2 = 0.02$ m and the initial free profile in the moonpool with $\eta = 0.02$ m, are adopted in the free decay tests. The time histories of heave motion responses and free surface oscillations are illustrated in Figure 8, including the corresponding spectrums by the Fast Fourier transform. In the results, the amplitudes of the heave motion response do not decrease much with the elapse of time. Correspondingly, the two peaks appear in the results of spectral analysis. Similar phenomena can also be found in the results of free surface oscillations in the figure, although it is not very remarkable. The above free decay tests are also adopted in Ding et al., 2022 and Jing et al., 2024, where the non-monotonic decrease of amplitudes in the time history and two peaks in the spectrums can also be found in their work.

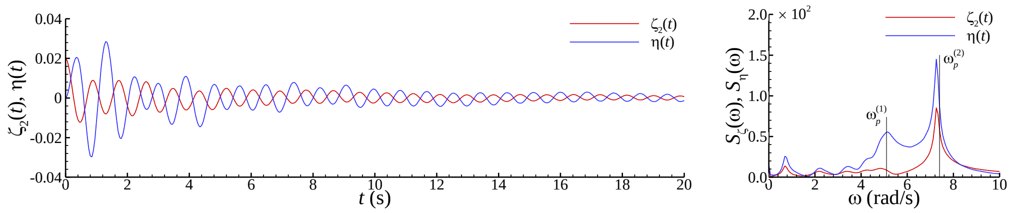

(a) Initial heave amplitude of the hulls with $\zeta_2 = 0.02$ m

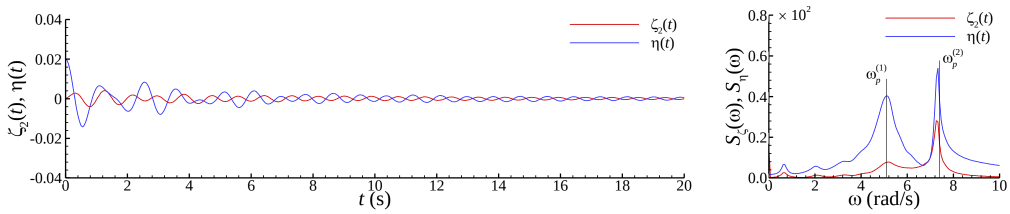

(b) Initial free profiles in the moonpool with $\eta = 0.02$ m

Figure 8: Time histories and corresponding spectrums of the traditional free decay tests.

Although the corresponding frequencies of two peaks can be observed, the time histories, in fact, are atypical in the above traditional free decay tests. This also indicates that the essential mechanics of the first and second resonant frequencies of the coupling system can not be revealed by the traditional free decay tests conducted above. In this study, a new approach to the free decay test is developed. Since the heave motion of the hulls and the fluid oscillation in the moonpool are a two-degree-of-freedom motion system, the in-phase and out-of-phase relationships between the heave motion displacement and the free surface profile are adopted as the initial state in the free decay test. That is, the in-phase initial state is heave displacement ζ_2 = 0.0072 m and free surface η = 0.0200 m; and the out-of-phase initial state is heave displacement ζ_2 = – 0.0094 m and free surface η = 0.0164 m. As shown in Figure 9, the amplitudes of heave motion and free surface oscillation decrease with the elapse of time in the time-varying results, including the in-phase and out-of-phase initial states. Correspondingly, the spectrums generally have a single peak. The free decay test with the in-phase initial state captures the first resonant frequency $\omega_p^{(1)}$ in Figure 9*a*, while the free decay test with the out-of-phase initial state obtains the second resonant frequency $\omega_p^{(2)}$ in Figure 9*b*. Furthermore, the in-phase initial state is able to generate the in-phase time histories of heave motion displacement and free surface profile in Figure 9*a*, while the out-of-phase initial state is able to generate the out-of-phase time histories in Figure 9*b*. All of these results confirm that the in-phase and out-of-phase relationships between the heave motion response of the hulls and the free surface oscillation in the moonpool are the first and second resonant modes of the coupled system, respectively.

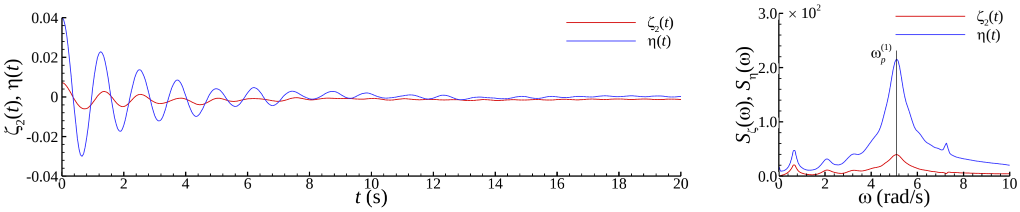

(a) In-phase initial states with ζ_2 = 0.0072 m and η = 0.04 m

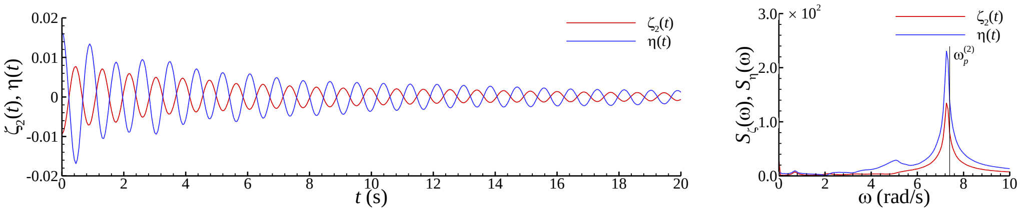

(b) Out-of-phase initial states with ζ_2 = - 0.0094 m and η = 0.0164 m

Figure 9: Time histories and corresponding spectrums of the new free decay tests.

Conclusions. The physics behind the two-peak response of the heave motion of the hulls coupling with the free surface oscillation in the moonpool is investigated. Theoretical analysis based on the potential flow model indicates that the two peaks correspond to the first and second resonant frequencies of the heave motion of the hulls with a moonpool. A conceptual model shows that the heave motion with the fluid oscillation system is essentially a two-degree-of-freedom motion system, where the heave motion of the hulls and the fluid oscillation in the moonpool are the main and attached spring oscillators, respectively. A new approach to the free decay test via CFD simulations is suggested, by which it is confirmed that the in-phase and out-of-phase relationships between the heave motion response of the hulls and the free surface oscillation in the moonpool are the first and second resonant modes of the coupled system, respectively.

Acknowledgments. This work is supported by the National Natural Science Foundation of China with Grant Nos. 52371267 and 52171250.

Declaration of interest. The authors report no conflict of interest.

References

Ding, Y., Walther, J. H. and Shao, Y. (2022). Higher-order gap resonance and heave response of two side-by-side barges under stokes and cnoidal waves, Ocean Engineering 266: 112835.

Gao, J., He, Z., Huang, X., Liu, Q., Zang, J. and Wang, G. (2021). Effects of free heave motion on wave resonance inside a narrow gap between two boxes under wave actions, Ocean Engineering 224: 108753.

Jiang, S.-C., Lan, J.-J., Bai, W. and Huang, Y.-Q. (2024). Coupling analysis between wave resonance in the moonpool and heave motion of the twin hulls with mooring effect, Physics of Fluids 36: 112102.

Jing, P., Cui, T., He, G., Zhang, C. and Luan, Z. (2024). Effects of multi motion responses and incident-wave height on the gap resonances in a moonpool, Physics of Fluids 36: 017117.

Lu, L., Tan, L., Zhou, Z., Zhao, M. and Ikoma, T. (2020). Two-dimensional numerical study of gap resonance coupling with motions of floating body moored close to a bottom-mounted wall, Physics of Fluids 32: 092101.

Newman, J. N. (1960). The exciting forces on fixed bodies in waves. Journal of Ship Research 6: 10-17.

Ravinthrakumar, S., Kristiansen, T., Molin, B. and Ommani, B. (2020). Coupled vessel and moonpool responses in regular and irregular waves, Applied Ocean Research 96: 102010.